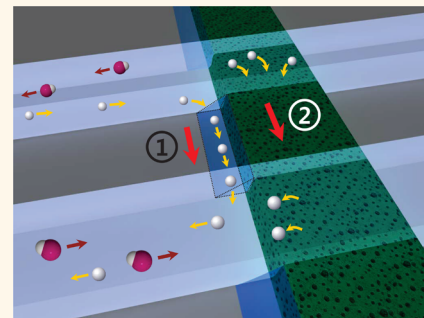


# Tunable Ionic Transport for a Triangular Nanochannel in a Polymeric Nanofluidic System

Bumjoo Kim,<sup>†</sup> Joonseong Heo,<sup>†</sup> Hyukjin J. Kwon,<sup>†</sup> Seong J. Cho,<sup>†</sup> Jongyoon Han,<sup>‡</sup> Sung Jae Kim,<sup>§,\*</sup> and Geunbae Lim<sup>†,✉,\*</sup>

<sup>†</sup>Department of Mechanical Engineering and <sup>‡</sup>Department of Integrative Bioscience and Biotechnology, Pohang University of Science and Technology, San 31, Pohang, Gyeongbuk, Korea, <sup>†</sup>Department of Electrical Engineering and Computer Science, Massachusetts Institute of Technology, 77 Massachusetts Avenue, Cambridge, Massachusetts 02139, United States, and <sup>§</sup>Department of Electrical and Computer Engineering and Inter-university Semiconductor Research Center, Seoul National University, 1 Gwanak-ro, Gwanak-gu, Seoul, Korea

**ABSTRACT** Recently, tremendous engineering applications utilizing new physics of nanoscale electrokinetics have been reported and their basic fundamentals are actively researched. In this work, we first report a simple and economic but reliable nanochannel fabrication technique, leading to a heterogeneously charged triangular nanochannel. The nanochannel utilized the elasticity of PDMS when it bonded with a micrometer-scale structure on a substrate. Second, we successfully demonstrated novel ionic transports by tweaking the micrometer structures: (1) the transition of nonlinear ionic conductance depending on the nanochannel properties and (2) the ionic field-effect transistor. Nanochannel conductance has two distinguishable nonlinear regimes called the “surface-charge-governed” and the “geometry-governed” regime and its only individual overviews were frequently reported. However, the transition between two regimes by adjusting nanochannel properties has not been reported due to the difficulty of functional nanochannel fabrication. In addition, a gate voltage was comfortably applied to the triangular nanochannel so that the field-effect ion transportation was reliably achieved. Therefore, presenting triangular nanochannels have critical advantages over its heterogeneous and tunable surface properties and thus, could be an effective means as an active fundamental to control and manipulate the ion-electromigration through a nanofluidic system.



**KEYWORDS:** triangular nanochannel · nanofluidics · ion concentration polarization · ionic conductance · ionic field-effect transistor

Recently, nanofluidic channels exhibit new physics that has never been realized in microfluidic systems such as nonconventional ionic transport,<sup>1</sup> nanocapillarity,<sup>2</sup> entropic trapping for DNA separation,<sup>3</sup> and ion concentration polarization due to electrical double layer overlap.<sup>4–8</sup> These scientific findings contributed to develop novel engineering applications in the form of nanofluidic diodes,<sup>9</sup> DNA manipulations in single nanochannels,<sup>10,11</sup> molecular preconcentrations<sup>12,13</sup> and desalination.<sup>14</sup> In this sense, nanofluidic channels become a fundamental and essential experimental platform to study nanoscale-molecular, -fluidic, and -ionic transport properties. In the beginning of the nanofluidic era, most of these nanofluidic channels were built on rigid substrates such as glass or silicon, utilizing standard microfabrication techniques in a clean room facility.<sup>3,15,16</sup> However, numerous research

groups have developed and fabricated different types of nanochannels using poly-(dimethylsiloxane) (PDMS),<sup>17–20</sup> thermoplastic materials<sup>21,22</sup> and polymeric membranes,<sup>14,23–28</sup> which can provide simple and cost-effective structures.

Indeed, a polymeric nanostructure, mainly Nafion (proton permeable membrane), has received wide attention as an attractive nanoporous material, since a nanoporous membrane fabrication process using Nafion does not require any nanolithographic tools or sophisticated manufacturing processes.<sup>23</sup> Instead, the polymeric network inside Nafion (randomly distributed pores at 1–100 nm) can easily form a nanoporous structure which would make it a perm-selective channel by itself. With the aid of polymeric nanoporous materials, various engineering applications have been successfully accomplished such as protein preconcentrator,<sup>23–28</sup> microfluidic

\* Address correspondence to limmems@postech.ac.kr, gates@snu.ac.kr.

Received for review October 30, 2012 and accepted December 5, 2012.

Published online December 17, 2012  
10.1021/nn3050424

© 2012 American Chemical Society

fuel cells,<sup>29</sup> and desalination<sup>14</sup> in the microfluidic chip. However, in this paper we reveal that nanofluidic phenomena, occurred in Nafion polymeric nanojunction systems, do not predominantly result from polymeric nanostructures by discovering the existence of hidden nanogaps; triangular shaped nanochannels next to the polymeric membrane. Definitely, previous researches using Nafion polymeric nanojunctions provide valuable results in points of science and engineering, even though their underlying mechanism for unique nanofluidic phenomena is somewhat incorrect.

Here, we report the unrevealed and hidden triangular nanochannel in polymeric nanofluidic systems and investigate its electrical behaviors as a functional nanochannel. Since the triangular nanochannel is composed of three different surface materials, that is, bottom glass substrate, top PDMS substrate, and thin membrane material, one can simply acquire unique and adjustable ionic transportation depending on various surface charge densities by changing the membrane materials as well as the geometry of the nanochannel by modifying membrane thickness. For example, the charge density of each surface would be dominant to ionic conductance at low electrolyte concentration (a.k.a. surface-charge-governed regime), while the size of the nanochannel would be dominant to ionic conductance at high electrolyte concentration (a.k.a. geometry-governed regime).<sup>15,16</sup> Thus we can exhibit the nonlinear conductance transition between two regimes at one time by modifying the thin membrane material and thickness. Furthermore, a nanofluidic field-effect-transistor, by depositing thin metal for applying gate voltages instead of the membrane, could be fabricated without any nanolithographical tools. Such versatility of the heterogeneous triangular nanochannel could provide an economic and reliable nanofluidic platform for novel engineering applications as well as fundamental researches.

## RESULTS AND DISCUSSION

To visibly verify the structural nanogap, a simple and typical microchannel–nanochannel junction is fabricated as shown in Figure 1a (see Supporting Information section 1). A PDMS microchannel is bonded to the slide glass substrate after a straight micropattern of a membrane with submicrometer thickness. The membrane material is chosen to be generally used in most researches concerning the polymeric nanochannel such as Nafion, oxide layer, etc. During the bonding process of the PDMS substrate with the glass substrate that has a thin polymeric nanojunction, one can assume that there is no structural gap or leakage at each end of nanojunction since the thickness of polymeric nanojunction is negligible (less than  $1\text{ }\mu\text{m}$ ) and PDMS has a unique flexibility (the shear modulus varies between 100 kPa and 3 MPa and the Young's modulus is 360–870 kPa; cf. the Young's modulus of PMMA is

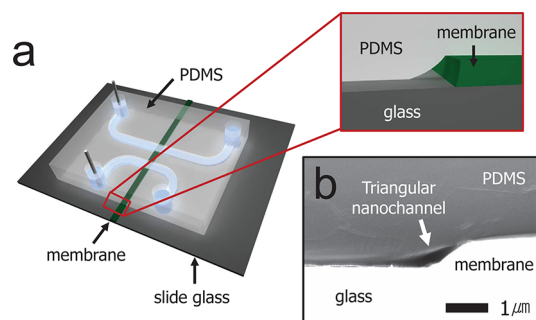


**Figure 1.** Triangular nanochannel scheme. Schematic illustration of (a) micro-/nanofluidic chip and magnified view of triangular nanochannel created by incomplete bonding with PDMS substrate. (b) SEM image of triangular nanochannel created by the membrane (500 nm height).

1800–3100 MPa).<sup>30</sup> However, there must be an incomplete bonding at the edges of the membrane due to the embossed pattern of the nanojunction. The created gaps have a nanoscale dimension with triangular shape as shown in the magnified schematics in Figure 1a. Especially, each wall of the gap is made of three different materials, PDMS, glass substrate, and membrane material. Figure 1b shows the SEM image of the triangular nanochannel, confirming the existence of these hidden nanochannels. Therefore, a prominent nanojunction or nanostructure enclosed by the PDMS lump could generate an unexpected structural nanogap, a so-called heterogeneous triangular nanochannel, in micro-/nanofluidic chips.

In the 2-dimensional micro-/nanohybrid system shown in Figure 2a which has been used for most applications, the electrical voltage was applied to two (or one) north poles, while the south pole was electrically grounded for flowing ionic current through the nanobridge. The polymeric nanojunction is known as the primary current path; however, the triangular nanogap could be the alternative current path. Therefore, on the basis of the additional existence of the triangular nanochannel, it is necessary to investigate whether the ionic current flows through either the nanojunction or the triangular nanochannel or both. To remove the inevitable triangular nanochannel and let ions flow only through the polymeric nanojunction, a portion of the PDMS substrate on the nanojunction between the main and buffer microchannel was mechanically punched out. Then uncured PDMS solution was poured into the hole so that the solution completely sealed around the membrane to prevent the formation of the triangular nanochannel (see Supporting Information section 2). Basic nanofluidic devices with and without triangular nanochannels were prepared for measuring ionic conductance as shown in Figure 2 panels b and c, respectively. Each nanojunction is fabricated on the glass substrate using the Nafion solution by the surface-patterned method,<sup>23</sup> but the device without a triangular nanochannel (Figure 2c) has post-PDMS

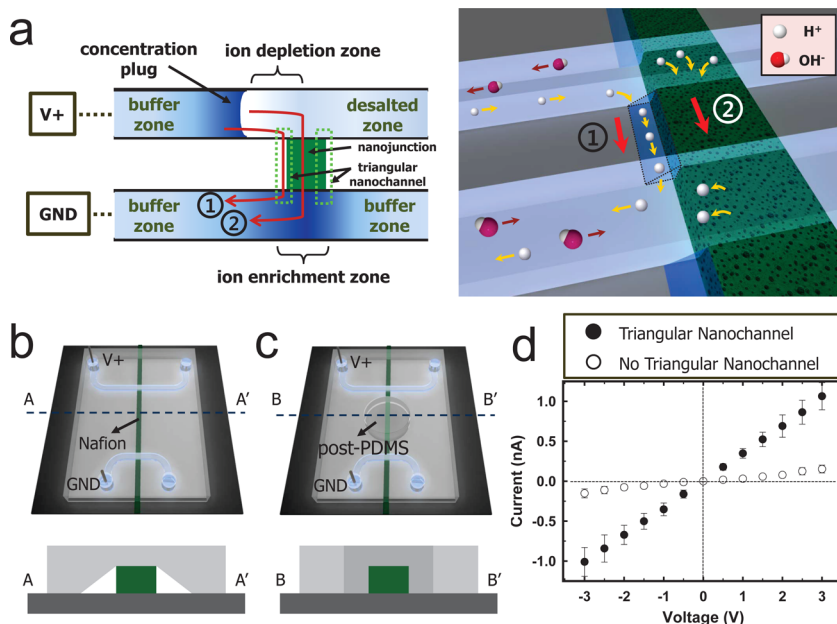


**Figure 2.** Ion transport through the polymeric nanojunction and triangular nanochannel. (a) Schematic illustrations of micro-/nanohybrid systems. There could be two ionic current paths through the polymeric nanojunction or triangular nanochannel. Schematics of prepared devices (b) with and (c) without the triangular nanochannel. A hole was made by mechanical punching between microchannels and pouring post-PDMS into the hole with the intention of removing the triangular nanochannel along the membrane material. Length and thickness of membrane across the microchannels is 5 mm and 1  $\mu\text{m}$ , respectively. The diameter of the hole is 3 mm. (d)  $I$ – $V$  characteristics of the device with/without triangular nanochannel; 1 mM KCl is used as buffer solution.

at the center of the device. For measuring ionic conductance across the nanojunction, both main (top microchannel) and buffer (bottom microchannel) channels are filled with 1 mM KCl solution, and DC voltage ( $V$ +) and ground (GND) is applied between the microchannels without external pressure. The applied voltage is step-changed from  $-3$  V to  $+3$  V with a sweep rate at 0.5 V/3 s. All experiments were repeated at least 20 times for accurate measurement. Figure 2d presents  $I$ – $V$  characteristics to show different ionic conductance depending on the existence of the triangular nanochannel. The conductance can be estimated from the slope of each  $I$ – $V$  line. Ionic conductance with a hole (0.35 nS), that is, with a triangular nanochannel, is significantly higher at more than 7 times those with a post-PDMS (0.047 nS), that is, without a triangular nanochannel. This result in turn shows that most ionic transports in micro-/nanofluidic chips using a polymeric nanojunction occur mainly through the hidden triangular nanochannel, not through the nanoporous polymeric junction. However, another point which should be considered is that ions also flow through the Nafion nanojunction though they are relatively small. According to the above experiments, therefore, it could be assumed that previous researches, which have studied various nanofluidic phenomena and effects using polymeric nanojunctions in a PDMS microchip, are based on ion transports not through the nanoporous junction but through the triangular nanochannel.

Although the above results could suggest important findings, additional investigation and crucial proof is

still needed for the role of triangular nanochannels in nanofluidic applications. The main reason that many researchers use the polymeric nanojunctions is to take advantage of its perm-selectivity (preferentially conducting ions with one polarity over another) that leads to a variety of nonlinear electrokinetic behaviors.<sup>5,8,12,13,31</sup> Consequently the perm-selectivity of the triangular nanochannel must be checked in addition to a comparison of electrical conductance shown in the previous section. Among the nanofluidic phenomena, an ion concentration polarization (ICP) could be an exact and direct clue of perm-selectivity, because it can provide both quantitative and qualitative values. The typical behavior of the ICP is to significantly decrease (or increase) the ion concentration in the anodic (or cathodic) end of the nanochannel so that the ion depletion (or enrichment) zone could be formed at the anodic (or cathodic) side in the case of cation-selective nanojunction.<sup>12</sup> With anion-selective nanojunction, the locations where the ion depletion occurs and the enrichment zone forms are switched.<sup>32</sup> By depositing a Nafion nanojunction with 1  $\mu\text{m}$  thickness across two microchannels, a typical nanofluidic device for the ICP experiment is fabricated as shown in Figure 3a. A 1 mM KCl solution is filled in both the main (top) and buffer (bottom) channels, and external DC voltage is applied across the Nafion nanojunction. In addition, 1  $\mu\text{g}/\text{mL}$  of fluorescein sodium salt solution (490 nm excitation and 520 nm emission) is used to observe flow field and ion behaviors. As expected, a fluorescent image clearly shows both an ion-depletion zone and

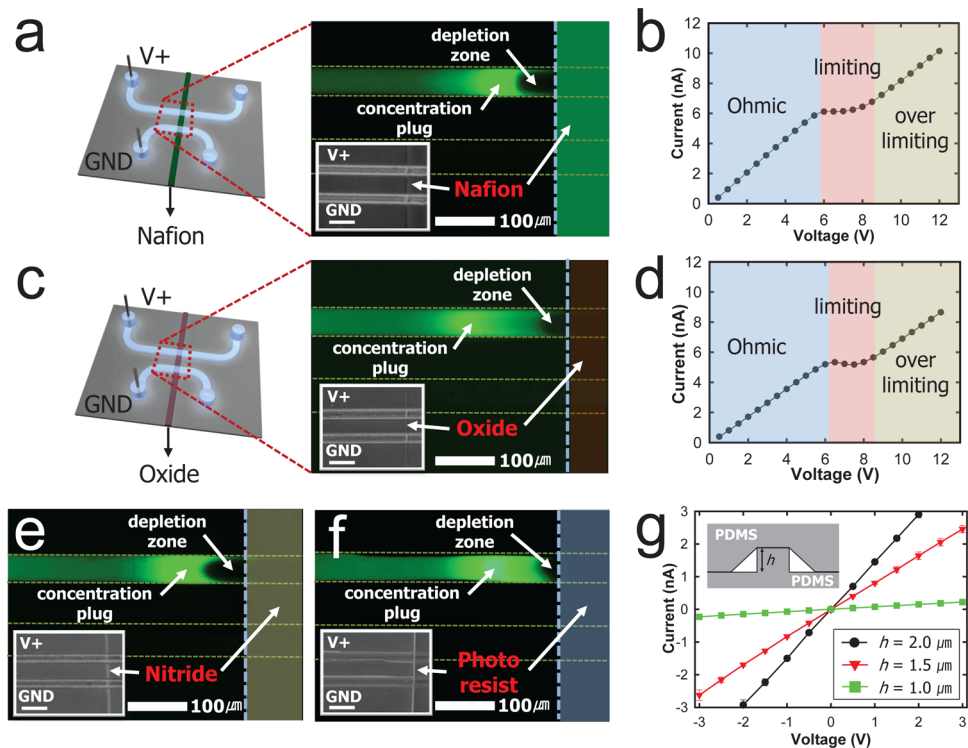


**Figure 3.** Perm-selectivity of the triangular nanochannel. Fluorescent images of the perm-selectivity test of ion concentration polarization (ICP) phenomena using (a) Nafion, (c) oxide ( $\text{SiO}_2$ ), (e) nitride ( $\text{SiN}_x$ ) and (f) photoresist (AZ GXR 601) film with  $1\text{ }\mu\text{m}$  thickness as membrane materials. Panels b and d represent  $I$ – $V$  characteristics using Nafion and oxide as membrane, respectively. Fluorescent images show that perm-selectivity driving ICP phenomena arises from a triangular nanochannel. Moreover, both  $I$ – $V$  curves clearly show Ohmic, limiting and overlimiting region sequentially which is a unique ICP characteristics. (g) Conductance measurement with various thicknesses of PDMS bumps to verify the repeatable nanochannel formation. The standard deviation for each thickness is less than 10% showing good fabrication reliability; 1 mM KCl is used as buffer solution in all experiments.

an ion-preconcentration plug around the anodic end of the nanojunction as shown in Figure 3a. Along with an observation of ion-depletion and the preconcentrated plug,  $I$ – $V$  characteristics for ICP phenomenon could also be found as shown in Figure 3b with linearly increased voltages at 0.5 V/5 s from 0 to 12 V. In general, when a perm-selective nanojunction leads ICP, a limiting and overlimiting current region should appear next to the Ohmic range due to initiation and development of an ion depletion zone which imposes a dynamic change of electrical resistance.<sup>5</sup> However, it could not be concluded whether Nafion or the triangular nanochannel has the perm-selectivity because Nafion is a highly conductive and proton permeable material as well. For identifying exclusive effects of a triangular nanochannel on ICP behaviors, an oxide ( $\text{SiO}_2$ ) layer known as nonconducting material with  $1\text{ }\mu\text{m}$  thickness is deposited on the slide glass substrate by PECVD instead of a Nafion nanojunction, while the other experimental conditions are kept to be the same. Figure 3c shows a fluorescent image presenting an oxide nanojunction that also exhibits ICP phenomena like a Nafion nanojunction. Moreover, as shown in Figure 3d, the  $I$ – $V$  characteristics of the oxide nanojunction are almost similar (slightly lower current level) with those of Nafion clearly showing a limiting and

overlimiting current region after 6 V. Since an ionic current still can be passed through the Nafion itself, the overall current level shown in Figure 3b should be higher than that of Figure 3d. These results absolutely can explain that a dominant perm-selectivity for ICP should be originated from not polymeric nanojunction but triangular nanochannel since it is impossible to generate ICP behaviors through nonconductive oxide nanojunction. Finally we repeated the above experiments with a thin nitride ( $\text{SiN}_x$ ) membrane and thin photoresist (AZ GXR 601) pattern under the same experimental conditions and acquired comparable results as shown in Figure 3e and 3f, respectively. Thus, one can conclude that the role of the triangular nanochannel is significant to initiating ICP (perm-selectivity) regardless of membrane materials. To verify the repeatable nanochannel formation, the conductance with various membrane thicknesses is measured as shown in Figure 3g. These tests utilize PDMS bumps for varying the membrane thickness. The standard deviation for each thickness is less than 10%, showing good fabrication reliability. Therefore, any quantification study could be done using the heterogeneous nanochannel regardless of the flexibility of PDMS material.

With regard to ion transport in nanofluidic channels, it is revealed that the conductance through the

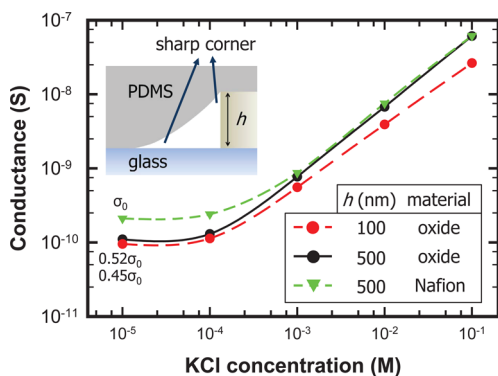


**Figure 4.** Ionic conductance characteristics of a triangular nanochannel. Conductance of various membrane materials and their height as a function of buffer concentration. The conductance of the nanochannel created by a 500 nm oxide membrane follows the surface-charge-governed region at low electrolyte concentration, while it reaches the geometry-governed region at high electrolyte concentration.

nanochannel is governed by surface charge at low ionic concentrations, while nanochannel geometry and bulk ionic concentration determine the conductance at high ionic concentration because of more severe electrical double layer overlap in lower ionic concentration.<sup>15,16</sup> Since the triangular nanochannel that we have found is enclosed by heterogeneous surface materials (PDMS, glass, and nanojunction material as shown in the inset of Figure 4), it is favorable to investigate the electrical behaviors by manipulating the membrane properties such as thickness and material itself. Nafion and oxide membranes with 500 nm thickness are prepared for surface charge effects at low electrolyte concentration, while a 100 nm thickness oxide membrane is prepared for nanochannel geometry effects at high electrolyte concentration simultaneously. KCl bulk concentrations are swept from 0.01 mM to 0.1 M for measurement of the  $I$ – $V$  curve in the Ohmic regime, and each experiment was repeated at least five times for reproducibility. Figure 4 clearly shows the effect of membrane properties on the nanochannel conductance. The thickness of electrical double layer is inversely proportional to the square root of the electrolyte concentration and typically is  $\sim 1$  nm at 100 mM concentration of a 1:1 electrolyte solution.<sup>33</sup> Thus, the electrical double layer overlaps should be obtained below 0.1 mM and 0.001 mM for the 100 nm and 500 nm nanochannels, respectively. However, the transition could occur around 1 mM concentration in real situations since (1) the partial perm-selective ion transportation can initiate an electrical double layer overlap and it accelerates perm-selectivity as a positive feedback loop<sup>5</sup> and (2) a thinner nanochannel can be created at the corners of the triangular cross-section and this promotes the electrical double layer overlap. In a comparison of the triangular nanochannel created by 100 nm oxide membrane (red dots) and 500 nm membrane (black dots), the conductance is almost similar at a low ionic concentration

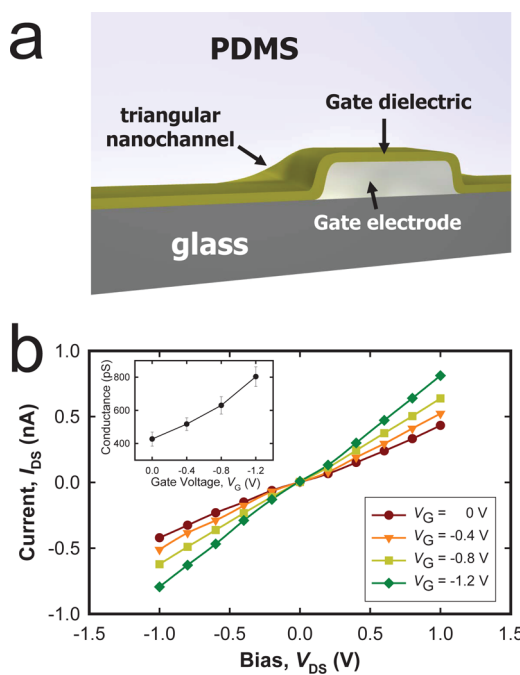


**Figure 5.** Nanofluidic field-effect-transistor using a triangular nanochannel. Schematic illustration of (a) nanofluidic FET system. (b) Representative current/bias ( $I_{DS}/V_{DS}$ ) curves recorded at different gate voltage,  $V_G$ . Inset plot shows a linear relationship between gate voltage and ionic conductance through the triangular nanochannel; 1 mM KCl is used as buffer solution.

(surface charge dominant region) because of the same oxide wall (*i.e.*, the same surface charge), while the difference becomes larger at higher ionic concentration (channel geometry and bulk concentration dominant region) due to the different nanochannel scale. On the other hand, in a comparison of the triangular nanochannel created by 500 nm oxide membrane (black dots) and 500 nm Nafion membrane (green dots), the conductance of Nafion is almost twice higher than that of oxide at low ionic concentration since Nafion has a higher surface charge than the oxide layer (see Supporting Information section 3), while they have similar conductance at high ionic concentration due to the same geometrical feature of a triangular nanochannel. Consequently, the nanochannel with a 500 nm oxide wall acts like a nanochannel with a 100 nm oxide wall at low concentration, whereas it acts like a 500 nm Nafion wall at high concentration. This is the first demonstration to definitely show the transition behavior of ionic conductance from surface-charge-governed regime to geometry-governed regime simultaneously and rigorously with the aid of the effective and easy control of nanochannel properties. Additionally it can be a direct clue showing that most ionic transport occurs through the triangular nanochannel composed of heterogeneous surface materials. On the basis of our results, it would be possible to achieve functional nanochannels with various conductance characteristics by changing the membrane materials and controlling channel geometry.

Moreover, the nanofluidic field-effect-transistor, which is capable of actively controlling the ion transportation by applying a gate voltage, is fabricated utilizing the heterogeneous nanochannel. Instead of a membrane on a glass substrate, gate electrodes are deposited with a dielectric layer as shown in Figure 5a. The heterogeneous triangular nanochannels are formed by the same manner, but the surface charge density (or zeta potential) on the dielectric layer can be easily controlled by applying the gate voltage at the gate electrode.<sup>9,34,35</sup> A typical fabrication process of an ionic field-effect transistor usually requires submicrometer nanochannel fabrication, gate electrode patterning, insulation layer deposition, and integration of all components which are critical nuisances for the advance of nanofluidic researches. On the contrary, our heterogeneous nanochannel dramatically reduces the process time/cost to accelerate researches in this field. In addition to this, since the gate electrode spans along the entire nanochannel surface, more accurate controls could be achieved in the heterogeneous nanochannel than the device which can control a surface charge only at specific locations along the nanochannel. As shown in Figure 5b,  $I_{DS}$ , the ionic currents from source to drain, are precisely controlled by  $V_G$ , the gate voltage at the subnano ampere level and the conductance of the nanochannel as well (see Supporting Information sections 4 and 5 for the experimental diagram of ionic field-effect-transistor and monitoring gate leakage current, respectively.)

## CONCLUSION

Here, we have unveiled the existence of a triangular nanochannel in a polymeric nanojunction system with a PDMS-enclosed micro/nanofluidic system. In addition, we have investigated nonlinear ionic conductance and perm-selectivity of a heterogeneous triangular nanochannel concluding that the unique nanoscale electrokinetic phenomena in a polymeric nanojunction platform mainly arise not through the nanoporous structure but through the triangular nanochannel. Finally on the basis of the nanochannel enclosed by the heterogeneous materials, we have clearly exhibited the nonlinear conductance transition from surface-charge-governed regime to geometry and bulk concentration

dominant regime at one time. Also, we have repeated all experiments, shown in this paper, with sodium phosphate, dibasic ( $\text{Na}_2\text{HPO}_4$ ) buffer solution in order to verify whether our results are applicable to general ionic solutions other than monovalent ionic solution. Lastly, we demonstrate the basic function of the ionic field-effect-transistor in an effective and economic manner using the gate electrode instead of sophisticated nanolithographical facilities. Conclusively these demonstrations confirm that a major electrical variation in one surface would control the whole device operation, though each surface has different surface charges. More importantly, the presenting triangular nanochannel has heterogeneous and tunable surfaces to archive this critical controllability.

The electrical conductivity of Nafion is known to be superior to that of the bulk solution used in this work.<sup>36</sup> Thus, it is still valid that most of the current tends to flow through the polymeric networks inside Nafion as shown in previously published papers.<sup>14,23–28</sup> However, ionic conductance inside the triangle nanochannel (because the conductance of electrical double layer is higher compared to the bulk solution where an electroneutrality is held) is higher than that of Nafion as confirmed in Figure 2. Therefore, the nonlinear electrokinetic flow generated along the Nafion membrane in most of the Nafion-based nanofluidic devices (see Figure 2 of ref 26) is coming from the fact that the ionic current from bulk solution should flow through the Nafion porous membrane first and then switch the current path along the triangular nanochannel.

We note that the triangular nanochannel is a highly attractive research subject for nanofluidic phenomena due to its cross-sectional geometry. Unlike a rectangular nanochannel, one triangular nanochannel is considered to be composed of various-sized parallel nanochannels (*i.e.*, a thin nanochannel at the corner of the triangle and a thick nanochannel at the center of triangle), which could give us controllability for ion transport and perm-selectivity by the scale of electrical double layer. Therefore, the functional triangular nanochannel that we have found must provide diverse challenges for nanofluidic phenomena in future applications such as nanofluidic integrated circuit, etc.

## METHODS

**Device Fabrication.** We fabricated Nafion nanojunction on the glass slide using previously published surface patterning methods.<sup>23</sup> First, using a dummy straight microchannel, Nafion solution (Nafion perfluorinated resin solution, 20 wt %, Sigma-Aldrich) was allowed to flow into the microchannel by applying negative pressure. After remove the microchannel, the Nafion stripe on the glass slide was annealed for 5 minutes at 95 °C on the hot plate to evaporate solvent immediately. Microchannel molds for Nafion patterning had dimensions of 100  $\mu\text{m}$  (width)  $\times$  15  $\mu\text{m}$  (depth) and 100  $\mu\text{m}$  (width)  $\times$  50  $\mu\text{m}$  (depth) for Nafion membrane thicknesses of 500 nm and 1  $\mu\text{m}$ , respectively.

The thicknesses of Nafion membrane were confirmed by Alpha step. All microchannels used in this work had dimensions of 50  $\mu\text{m}$  (width)  $\times$  15  $\mu\text{m}$  (depth). To fabricate the oxide and nitride nanojunctions, the oxide layer and nitride layer (thickness of 100, 500, or 1000 nm) were deposited on slide glass by PECVD and a straight pattern (width of 100  $\mu\text{m}$ ) was created by RIE. The photoresist strips were photolithographically patterned after spin coating AZ GXR 601 on the slide glass. The test microchannels in PDMS were then bonded with the slide glass by plasma treatment (Cute-MP, Femto Science, Korea). Assembled chips were baked for 1 h at 70 °C on the hot plate for a secure bond. The main and buffer microchannel had dimensions of 50  $\mu\text{m}$  (width)  $\times$  15  $\mu\text{m}$  (depth)

and the distance between two channels was  $60\text{ }\mu\text{m}$ , except for that in the experiments shown in Figure 2 (distance was 5 mm). We mechanically punched the hole shown in Figure 2 before the PDMS was bonded to the glass substrate. For a field-effect transistor, aluminum of 700 nm thickness was deposited on Pyrex glass by sputtering, followed by 10 nm of a dielectric insulation layer ( $\text{HfO}_2$ ) by atomic layer deposition (NCD Corp., Lucida D100). After deposition, the PDMS microchannels were bonded.

**Materials.** The main buffers of KCl (Sigma Aldrich) and  $\text{Na}_2\text{HPO}_4$  (Sigma Aldrich) were prepared at various concentrations. For visualizing flow patterns and the depletion zone, fluorescein sodium salt ( $1\text{ }\mu\text{g/mL}$ , Sigma Aldrich, 490 nm excitation and 520 nm emission) was added to the main buffers.

**Methods.** Ionic currents through fabricated triangular nanochannels were measured using a source measurement unit (Keithley 238) from  $-3\text{ V}$  to  $3\text{ V}$  at  $0.5\text{ V/3 s}$  rate. Ionic conductance at each electrolyte concentration was calculated from the slope of this IV curve. For tracking the depletion zone and concentrated plus, we used an inverted fluorescent microscope (Olympus IX71) and a CCD camera (Olympus DP 72). Open source software, ImageJ was used for image analysis. IV sweep plots were obtained by the same power source from 0 to  $12\text{ V}$  at  $0.5\text{ V/5 s}$  rate. All measurements were repeated at least 20 times for confirming repeatability. For FET tests, a dual channel source measurement unit (Keithley 2636A) was used for applying voltages to drain, source, and gate and measuring each current. The specific experimental setup is shown in Supporting Information section 4.

**Conflict of Interest:** The authors declare no competing financial interest.

**Acknowledgment.** We gratefully acknowledge the financial support of a National Research Foundation grant, Mid-Career Researcher Program, funded by Korea Ministry of Education, Science and Technology (No. 2012R1A1A2007580). We also thank Dr. Jongyuk Son and Dr. Chulhwan Kim for KPFM measurements and Mr. Kumjae Shin for FET measurements. S. J. Kim was partially supported by the Future-Based Technology Development Program (Nano Fields) through NRF funded by the MEST (No. 2012-0001033).

**Supporting Information Available:** Additional figures as described in the text. This material is available free of charge via the Internet at <http://pubs.acs.org>.

## REFERENCES AND NOTES

1. Daiguji, H. Ion Transport in Nanofluidic Channels. *Chem. Soc. Rev.* **2010**, *39*, 901–911.
2. Honschoten, J. W.; Brunets, N.; Tas, N. R. Capillarity at the Nanoscale. *Chem. Soc. Rev.* **2010**, *39*, 1096–1114.
3. Han, J.; Craighead, H. G. Separation of Long DNA Molecules in a Microfabricated Entropic Trap Array. *Science* **2000**, *288*, 1026–1029.
4. Wang, Y. C.; Stevens, A. L.; Han, J. Million-fold Preconcentration of Proteins and Peptides by Nanofluidic Filter. *Anal. Chem.* **2005**, *77*, 4293–4299.
5. Kim, S. J.; Wang, Y. C.; Lee, J. H.; Jang, H.; Han, J. Concentration Polarization and Nonlinear Electrokinetic Flow near a Nanofluidic Channel. *Phys. Rev. Lett.* **2007**, *99*, 044501.
6. Pu, Q.; Yun, J.; Temkin, H.; Liu, S. Ion-Enrichment and Ion-Depletion Effect of Nanochannel Structures. *Nano Lett.* **2004**, *4*, 1099–1103.
7. Plecic, A.; Schoch, R. B.; Renaud, P. Ionic Transport Phenomena in Nanofluidics: Experimental and Theoretical Study of the Exclusion-Enrichment Effect on a Chip. *Nano Lett.* **2005**, *5*, 1147–1155.
8. Kim, S. J.; Li, L. D.; Han, J. Amplified Electrokinetic Response by Concentration Polarization near Nanofluidic Channel. *Langmuir* **2009**, *25*, 7759–7765.
9. Cheng, L. J.; Guo, L. J. Nanofluidic Diodes. *Chem. Soc. Rev.* **2010**, *39*, 923–938.
10. Levy, S. L.; Craighead, H. G. DNA Manipulation, Sorting, and Mapping in Nanofluidic Systems. *Chem. Soc. Rev.* **2010**, *39*, 1133–1152.
11. Persson, F.; Tegenfeldt, J. O. DNA in Nanochannels—Directly Visualizing Genomic Information. *Chem. Soc. Rev.* **2010**, *39*, 985–999.
12. Kim, S. J.; Song, Y. A.; Han, J. Nanofluidic Concentration Devices for Biomolecules Utilizing Ion Concentration Polarization: Theory, Fabrication, and Applications. *Chem. Soc. Rev.* **2010**, *39*, 912–922.
13. Zangle, T. A.; Mani, A.; Santiago, J. G. Theory and Experiments of Concentration Polarization and Ion Focusing at Microchannel and Nanochannel Interfaces. *Chem. Soc. Rev.* **2010**, *39*, 1014–1035.
14. Kim, S. J.; Ko, S. H.; Kang, K. H.; Han, J. Direct Seawater Desalination by Ion Concentration Polarization. *Nat. Nanotechnol.* **2010**, *5*, 297–301.
15. Stein, D.; Kruithof, M.; Dekker, C. Surface-Charge-Governed Ion Transport in Nanofluidic Channels. *Phys. Rev. Lett.* **2004**, *93*, 035901.
16. Karnik, R.; Castelino, K.; Fan, R.; Yang, P.; Majumdar, A. Effects of Biological Reactions and Modifications on Conductance of Nanofluidic Channels. *Nano Lett.* **2005**, *5*, 1638–1642.
17. Huh, D.; Mills, K. L.; Zhu, X.; Burns, M.; Thouless, M. D.; Takayama, S. Tuneable Elastomeric Nanochannels for Nanofluidic Manipulation. *Nat. Mater.* **2007**, *6*, 424–428.
18. Chung, S.; Lee, J. H.; Moon, M. W.; Han, J.; Kamm, R. D. Non-lithographic Wrinkle Nanochannels for Protein Preconcentration. *Adv. Mater.* **2008**, *20*, 3011–3016.
19. Park, S. M.; Huh, Y. S.; Craighead, H. G.; Erickson, D. A Method for Nanofluidic Device Prototyping Using Elastomeric Collapse. *Proc. Natl. Acad. Sci. U.S.A.* **2009**, *106*, 15549–15554.
20. Park, K. D.; Lee, S. W.; Takama, N.; Fujii, T.; Kim, B. J. Arbitrary-Shaped Nanochannels Fabricated by Polymeric Deformation to Achieve Single DNA Stretching. *Microelectron. Eng.* **2009**, *86*, 1385–1388.
21. Shao, P. E.; Kan, A.; Wang, L. P.; Ansari, K.; Bettoli, A. A.; Watt, F. Fabrication of Enclosed Nanochannels in Poly(methylmethacrylate) Using Proton Beam Writing and Thermal Bonding. *Appl. Phys. Lett.* **2006**, *88*, 093515.
22. Ionescu, R. E.; Marks, R. S.; Gheber, L. A. Manufacturing of Nanochannels with Controlled Dimensions Using Protease Nanolithography. *Nano Lett.* **2005**, *5*, 821–827.
23. Lee, J. H.; Song, Y. A.; Han, J. Multiplexed Proteomic Sample Preconcentration Device Using Surface-Patterned Ion-Selective Membrane. *Lab Chip* **2008**, *8*, 596–601.
24. Lee, J. H.; Cosgrove, B. D.; Lauffenburger, D. A.; Han, J. Microfluidic Concentration-Enhanced Cellular Kinase Activity Assay. *J. Am. Chem. Soc.* **2009**, *131*, 10340–10341.
25. Chen, C. H.; Sakar, A.; Song, Y. A.; Miller, M. A.; Kim, S. J.; Griffith, L. G.; Lauffenburger, D. A.; Han, J. Enhancing Protease Activity Assay in Droplet-Based Microfluidics Using a Biomolecule Concentrator. *J. Am. Chem. Soc.* **2011**, *133*, 10368–10371.
26. Kwak, R.; Kim, S. J.; Han, J. Continuous-flow Biomolecule and Cell Concentrator by Ion Concentration Polarization. *Anal. Chem.* **2011**, *83*, 7348–7355.
27. Cheow, L. F.; Han, J. Continuous Signal Enhancement for Sensitive Aptamer Affinity Probe Electrophoresis Assay Using Electrokinetic Concentration. *Anal. Chem.* **2011**, *83*, 7086–7093.
28. Ko, S. H.; Kim, S. J.; Cheow, L. F.; Kang, K. H.; Han, J. Massively Parallel Concentration Device for Multiplexed Immunoassays. *Lab Chip* **2011**, *11*, 1351–1358.
29. Song, Y. A.; Batista, C.; Sarapeshkar, R.; Han, J. Rapid Fabrication of Microfluidic Polymer Electrolyte Membrane Fuel Cell in PDMS by Surface Patterning of Perfluorinated Ion-Exchange Resin. *J. Power Sources* **2008**, *183*, 674–677.
30. Mark, J. A. *Polymer Data Handbook*; Oxford University: New York, 1999.
31. Rubinstein, S. M.; MAnukyan, G.; Staicu, A.; Rubinstein, I.; Zaltzman, B.; Lammertink, R. G. H.; Mugele, F.; Wessling, M. Direct Observation of a Nonequilibrium Electro-osmotic Instability. *Phys. Rev. Lett.* **2008**, *101*, 236101.
32. Kim, P.; Kim, S. J.; Han, J.; Suh, K. Stabilization of Ion Concentration Polarization Using a Heterogeneous Nanoporous Junction. *Nano Lett.* **2010**, *10*, 16–23.

33. Probstein, R. F. *Physicochemical Hydrodynamics: An Introduction*; Wiley-Interscience: Hoboken, NJ, 1994.
34. Hu, N.; Ai, Y.; Qian, S. Field Effect Control of Electrokinetic Transport in Micro/nanofluidics. *Sens. Actuators B* **2012**, *161*, 1150–1167.
35. Siwy, Z. S.; Howorka, S. Engineered Voltage-Responsive Nanopores. *Chem. Soc. Rev.* **2010**, *39*, 1115–1132.
36. Slade, S.; Campbell, S. A.; Ralph, T. R.; Walsh, F. C. Ionic Conductivity of an Extruded Nafion 1100 EW Series of Membranes. *J. Electrochem. Soc.* **2002**, *149*, A1556–A1564.